

Lattice Genons

Zhao Liu,¹ Gunnar Möller,^{2,3,*} and Emil J. Bergholtz^{4,†}

¹*Dahlem Center for Complex Quantum Systems and Institut für Theoretische Physik,
Freie Universität Berlin, Arnimallee 14, 14195 Berlin, Germany*

²*Functional Materials Group, School of Physical Sciences, University of Kent, Kent CT2 7NZ, United Kingdom*

³*TCM Group, Cavendish Laboratory, University of Cambridge, Cambridge CB3 0HE, United Kingdom*

⁴*Department of Physics, Stockholm University, AlbaNova University Center, 106 91 Stockholm, Sweden*

(Dated: December 14, 2024)

We investigate extrinsic wormhole-like defects that effectively increase the genus of space in lattice versions of multi-component fractional quantum Hall systems. Although the original band structure is distorted by these defects, leading to localized midgap states, we find that a new lowest flat band representing a higher genus system can be engineered by tuning local single-particle potentials. Remarkably, once local many-body interactions in this new band are switched on, we identify various Abelian and non-Abelian fractional quantum Hall states, whose ground-state degeneracy increases with the number of defects, i.e. with the genus of space. This sensitivity of topological degeneracy to defects provides a “proof of concept” demonstration that genons, predicted by topological field theory as exotic non-Abelian defects tied to a varying topology of space, do exist in realistic microscopic models. Specifically, our results indicate that genons can be created in the laboratory by combining the physics of artificial gauge fields in cold atom systems with already existing holographic beam shaping methods for creating wormhole-like defects.

PACS numbers: 73.43.Cd, 71.10.Pm, 05.30.Pr

Introduction. Extrinsic defects embedded in topologically ordered phases of matter [1–5] may acquire exotic properties [6–20]. Genons [11, 12], named after their ability to effectively increase the genus of space thus enhancing the topological degeneracy, are particularly intriguing representatives of this idea and can be visualized as wormhole-like defects connecting separate “universes” of different components in the host system. Importantly, the linkage of genons to the topology of space and the underlying topological order establishes them as powerful tools to overcome the long standing challenge of accessing topological orders with tunable topology of space. It also imparts them with nontrivial quantum dimensions and braiding statistics that are significantly different from those of intrinsic quasiparticles of the host system [12], thus enabling fault tolerant topological quantum computation [21, 22] even in Abelian host states without this capability and extending our knowledge of topological order. However, while the beautiful idea of genons is based on effective topological field theory [11, 12] and corroborated by complicated exactly solvable models [6, 10, 15], its actual relevance to realistic microscopic models has remained open.

In this Letter, we fill this void by presenting the first evidence of genons in a microscopic lattice model which can favor lattice versions of fractional quantum Hall states, i.e., fractional Chern insulators [23, 24], and naturally host defects. We design a scheme to offset the negative influence of defects on the band structure to stabilize topological states. With compelling results from computer simulations based on exact diagonalization, we explicitly demonstrate the remarkable fingerprint of genons—the nontrivial dependence of the ground-state topological degeneracy on the number of defects that effectively tune the genus of space to high numbers. Our results provide a deep insight into the physical realization of genons in simple lattice models involving only single-particle

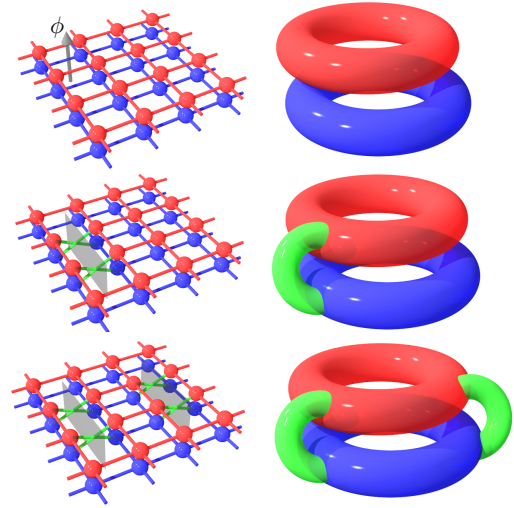


Figure 1. Our model is equivalent to two square lattice layers (blue and red) where each plaquette is pierced by an effective flux ϕ (upper left panel). We only plot nearest-neighbor hopping for simplicity. Defects are introduced through branch cuts (transparent grey) where the particles switch layer through wormholes (green). We study systems with up to two such branch cuts corresponding to the topologies displayed in the right panel.

hopping and onsite two-body interactions, thus opening the experimental accessibility of topological orders on high-genus surfaces.

Model. We consider a two-dimensional square lattice with two internal degrees of freedom $\sigma = \uparrow, \downarrow$ on each lattice site and an effective magnetic flux ϕ piercing each elementary plaquette (Fig. 1). For convenience, we refer to the internal degree of freedom as “layer”. We introduce a specific class of

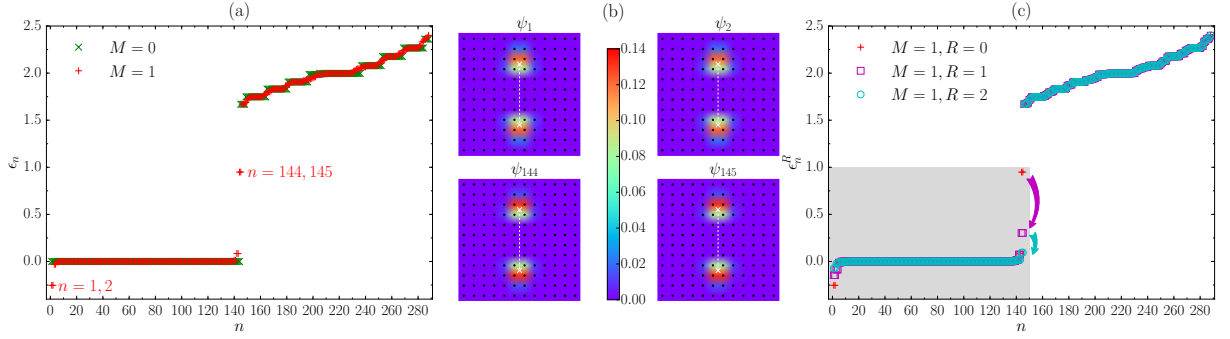


Figure 2. Band structure for a $L_x \times L_y = 12 \times 12$ lattice with $\phi = 1/2$. (a) The single-particle spectrum $\{\epsilon_n\}$ of H_0 . In the absence of defects ($M = 0$), $\epsilon_1, \dots, \epsilon_{144}$ are exactly degenerate at zero energy. With one branch cut ($M = 1$, white dashed line) at $(5.5, 2.5 \rightarrow 8.5)$, the original band structure is distorted, with two nearly degenerate clusters (ϵ_1, ϵ_2) and $(\epsilon_{144}, \epsilon_{145})$ having the largest deviation. (b) The lattice site weight of eigenvectors $\psi_1, \psi_2, \psi_{144}, \psi_{145}$ of H_0 for the same defects as in (a). All of them are strongly localized near the defects. The eigenstates with less energy deviation from the original band structure, for example, $\psi_3, \psi_4, \psi_{142}, \psi_{143}$, are less localized (not shown here). (c) The single-particle spectrum $\{\epsilon_n^R\}$ of $H_0 + V$ with $R = 0, 1$, and 2 and the same defects as in (a). $\epsilon_1^R, \dots, \epsilon_{145}^R$ which we must flatten (shaded in gray) becomes more degenerate for larger R , with the flatness 0.6, 3.1, 9.4 for $R = 0, 1, 2$.

defects into the lattice, which can be considered as \mathbb{Z}_2 twist defects [12] in the sense that a particle's layer index is flipped when it moves around such a defect once. It is helpful to imagine that the layer flipping occurs precisely along a branch cut connecting a pair of defects (Fig. 1). In case a straight hopping line intersects with n branch cuts, the particle flips its layer index n times.

We formulate the single-particle tight-binding Hamiltonian as

$$H_0 = \sum_{j,k,\sigma} t(z_j, z_k) a_{j, \mathcal{F}^{n_{jk}}(\sigma)}^\dagger a_{k,\sigma}, \quad (1)$$

where $a_{j,\sigma}^\dagger$ ($a_{j,\sigma}$) creates (annihilates) a particle in layer σ at lattice site j with coordinate $z_j = x_j + iy_j$, and $\mathcal{F}^{n_{jk}}(\sigma)$ flips σ for n_{jk} times if the hopping from z_k to z_j intersects with n_{jk} branch cuts. The hopping coefficient from z_k to z_j is designed as $t(z_j, z_k) = (-1)^{x+y+xy} e^{-\frac{\phi}{2}(1-\phi)|z|^2} e^{-i\pi\phi(x_j+x_k)y}$ [25, 26], where $z = z_j - z_k = x + iy$. Such a hopping is local in the sense that $t(z_j, z_k)$ follows a super-exponential decay. We focus on $\phi = 1/q$ with integer q , for which a unit cell contains q sites in the x -direction. In the absence of lattice defects, H_0 has a \mathbb{Z}_2 symmetry associated with exchanging the two layers and corresponds to two decoupled Kapit-Mueller models [25] in the Landau gauge, thus its lowest band structure contains two copies of an exactly flat band at zero energy with Chern number $\mathcal{C} = 1$.

The topology of our model strongly depends on the number of branch cuts (Fig. 1). If each layer has a torus geometry, each branch cut plays a role of a wormhole connecting two tori [11], hence the presence of M branch cuts leads to a surface with genus $g = M + 1$. In the following, we arrange the branch cuts in the y -direction without loss of generality [27], denoting the branch cut connecting a pair of defects at (X_1, Y_1) and (X_1, Y_2) as $(X_1, Y_1 \rightarrow Y_2)$. We also keep defects well separated from each other and avoid overlaps between branch cuts and lattice sites.

Single-particle spectra and defect-induced localized states.

We diagonalize H_0 on a periodic lattice \mathcal{L} of $L_x \times L_y$ sites to analyze the effect of defects on the band structure. We assume that L_x is divisible by q ensuring integer number of unit cells in the x -direction. In the absence of defects, the lowest $2\phi L_x L_y$ single-particle energy levels are exactly degenerate at zero energy. Such a flatness is seriously distorted when M pairs of defects are present, and we identify $4M$ levels with the most significant deviation from the original band structure: $2M$ of them (levels $\epsilon_1, \dots, \epsilon_{2M}$) drop below the original lowest band, and another $2M$ ($\epsilon_{2\phi L_x L_y - M + 1}, \dots, \epsilon_{2\phi L_x L_y + M}$) move into the original lowest band gap. Moreover, they form nearly degenerate clusters respectively. An example of the band structure for $M = 1$ is shown in Fig. 2(a). We further examine the eigenvectors of these $4M$ levels. Remarkably, we find that all of them are strongly localized near the defects [Fig. 2(b)], and the localization becomes weaker (or completely disappears) for other levels with less deviation from the original band structure. This localization enables us to do a controlled tuning of deviated energies by local potentials near the defects without significantly distorting the rest of the band structure, as we explain below.

Higher genus flat bands. Tuning deviated energies to recover a flat lowest band is necessary for stabilizing the many-body topological states. We consider $N_b = \frac{k}{2}(2\phi L_x L_y)$ bosons interacting via $(k + 1)$ -body onsite repulsions

$$H_{\text{int}} = \sum_{i \in \mathcal{L}, \sigma = \uparrow, \downarrow} : n_{i,\sigma} n_{i,\sigma} \cdots n_{i,\sigma} : \quad (2)$$

where $k \geq 1$ is an integer. In this setup, the ground state in the absence of defects is two copies of model \mathcal{Z}_k Read-Rezayi (RR) states on the lattice, which reside in the lowest $2\phi L_x L_y$ exactly degenerate eigenstates of H_0 with filling fraction $\nu = N_b / (2\phi L_x L_y) = k/2$ [28, 29]. Adding defects should not change the filling fraction in the thermodynamic limit, hence the most promising candidate of the ground

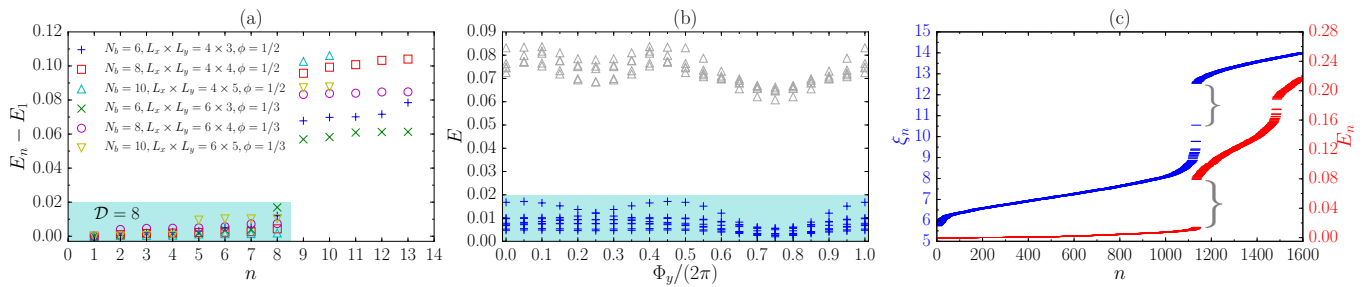


Figure 3. Defect-enhanced topological degeneracy for Abelian systems at $\nu = 1/2$. Two branch cuts are located at $(0.5, 0.25 \rightarrow 1.75), (2.5, 0.25 \rightarrow 1.75)$ for $L_x \times L_y = 4 \times 3$; $(0.5, 0.5 \rightarrow 2.5), (2.5, 0.5 \rightarrow 2.5)$ for $L_x \times L_y = 4 \times 4$ and 4×5 ; $(0.25, 0.25 \rightarrow 1.75), (3.25, 0.25 \rightarrow 1.75)$ for $L_x \times L_y = 6 \times 3$; $(0.25, 0.5 \rightarrow 2.5), (3.25, 0.5 \rightarrow 2.5)$ for $L_x \times L_y = 6 \times 4$; and $(0.25, 0.75 \rightarrow 3.25), (3.25, 0.75 \rightarrow 3.25)$ for $L_x \times L_y = 6 \times 5$. (a) The energy spectra of various system sizes. The eight quasi-degenerate ground states are highlighted by the cyan shade. (b) The y -direction spectral flow for $N_b = 6, L_x \times L_y = 4 \times 3, \phi = 1/2$. The eight ground states (blue +) never mix with excited states (gray Δ). (c) The PES (blue) for $N_b = 8, L_x \times L_y = 6 \times 4, \phi = 1/3$ in the $N_b^A = 4$ sector and the corresponding quasihole excitations (red) for $N_b = 4, L_x \times L_y = 6 \times 4, \phi = 1/3$. The number of states below the gaps (indicated by gray $\}$) are identical in both spectra.

state for M pairs of defects is the \mathcal{Z}_k RR state on a single $g = M+1$ surface, residing in the lowest N_s eigenstates of H_0 with the same filling fraction $\nu = \lim_{N_b \rightarrow \infty} N_b/N_s = k/2$. In accordance with this we target

$$N_s = 2N_b/k - (1 - g) \quad (3)$$

which also agrees with the continuum prediction in the lowest Landau level [30, 31]. The extra offset $1 - g$ is related to a topological quantity called the “shift”. To amplify the effect of the interaction, we consider the limit of N_s degenerate eigenstates. More precisely, in the presence of M pairs of defects, Eq. (3) requires us to flatten the energy dispersion of the lowest $N_s = 2N_b/k + M = 2\phi L_x L_y + M$ eigenstates of H_0 . This can be readily achieved by local perturbations owing to the strong localization of the deviated states near the defects [Fig. 2(a)]. A simple candidate of such a local potential is $V = -\sum_{n=1}^{2\phi L_x L_y + M} \epsilon_n \mathcal{T}_R(|\psi_n\rangle\langle\psi_n|)$, where ϵ_n ’s and ψ_n ’s are the eigenvalues and eigenvectors of H_0 respectively, and \mathcal{T}_R is the truncation at a radius R around each defect. The dominant terms in V exactly correspond to the localized eigenstates of H_0 whose energy dispersion we want to flatten, because other eigenstates staying at $\epsilon_n = 0$ have no contributions to V . This flattening process by V is asymptotically exact in the sense that the lowest $2\phi L_x L_y + M$ eigenstates of $H_0 + V$ at $R \rightarrow \infty$ will become exactly degenerate again at zero energy and have the same eigenvectors as those of H_0 . Remarkably, a very small R is already sufficient to do the flattening very well, with negligible influence on the pertinent eigenvector subspace. In Fig. 2(c), we show the band structure $\{\epsilon_n^R\}$ of $H_0 + V$ with $M = 1$ and $R = 0, 1, 2$ respectively. The degeneracy between the lowest $2\phi L_x L_y + M$ energy levels indeed becomes better with the increase of R , with the flatness $(\epsilon_{2\phi L_x L_y + M+1}^R - \epsilon_{2\phi L_x L_y + M}^R)/(\epsilon_{2\phi L_x L_y + M}^R - \epsilon_1^R)$ significantly increased to ≈ 9.4 for $R = 2$. The corresponding eigenvectors of $H_0 + V$ have a total 99% overlap with those of H_0 for $R = 1$ and $R = 2$.

Defect-enhanced topological degeneracy. After ensuring that a new lowest flat band can be recovered, we are now in the position to examine whether interactions can stabilize the \mathcal{Z}_k RR states in the single high-genus surfaces created in our model, by tracking the evolution of ground-state degeneracy \mathcal{D} with g [32]. We project the interaction H_{int} , which is assumed to be small relative to the band gap, to the lowest $2\phi L_x L_y + M$ eigenstates of H_0 [33] and neglect their energy dispersion for large numerical efficiency. This procedure is similar to the band projection in the flat-band limit which has been extensively used in previous studies of fractional Chern insulators without defects [34].

We first consider the most realistic $k = 1$ case. In the absence of defects, the ground state is two copies of $\nu = 1/2$ Laughlin states on the torus with degeneracy $\mathcal{D} = 2 \times 2 = 4$. After adding one pair of defects, we again get four-fold ground-state degeneracy, which is consistent with the $\nu = 1/2$ Laughlin state on a single $g = 2$ surface. A nontrivial enhancement of the topological degeneracy from $\mathcal{D} = 4$ to $\mathcal{D} = 8$ occurs for two pairs of defects ($g = 3$), characterized by eight approximately degenerate ground states for various system sizes [Fig. 3(a)]. These states are separated from other excited states by an energy gap which is significantly larger than the ground-state splitting, and the splitting is reduced relative to the excitation gap as the system size – and thus the separation of defects – is increased. We confirm the robustness of the topological degeneracy by the spectral flow [Fig. 3(b)]: we confirm that the eight ground states never mix with other excited states under twisted boundary conditions [26]. In order to further corroborate the topological nature of these ground states, we compute their particle entanglement spectra (PES) [34–37] to probe the quasihole excitation property. We do find a clear gap in the PES, the number of states below which is exactly the same as the corresponding counting of quasihole excitations [Fig. 3(c)] [34, 37]. Our evidence unambiguously indicates that the ground state in the presence of M pairs of defects is the $\nu = 1/2$ Laughlin state on a single

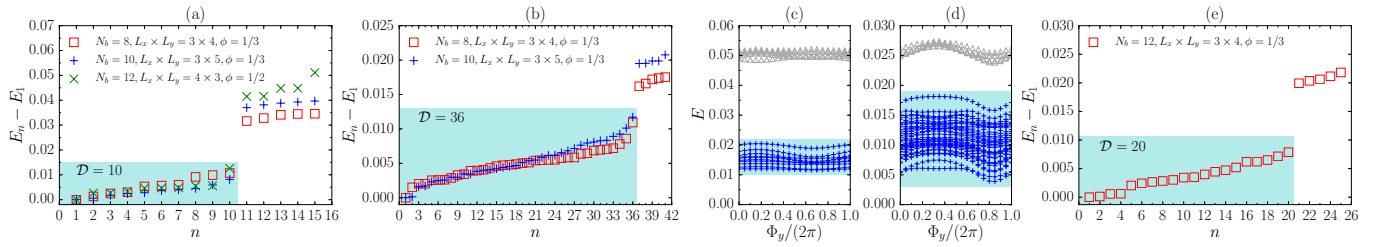


Figure 4. Defect-enhanced topological degeneracy for non-Abelian systems. The approximately degenerate ground states, together with the degeneracy \mathcal{D} , are highlighted by the cyan shade. (a) The energy spectra at $\nu = 1$ with one pair of defects. The branch cut is located at $(0.5, 0.5 \rightarrow 2.5)$ for $L_x \times L_y = 3 \times 4$; $(0.5, 0.75 \rightarrow 3.25)$ for $L_x \times L_y = 3 \times 5$; and $(1.5, 0.25 \rightarrow 1.75)$ for $L_x \times L_y = 4 \times 3$. (b) The energy spectra at $\nu = 1$ with two pairs of defects. The branch cuts are located at $(0.25, 0.5 \rightarrow 2.5)$, $(1.75, 0.5 \rightarrow 2.5)$ for $L_x \times L_y = 3 \times 4$ and $(0.25, 0.75 \rightarrow 3.25)$, $(1.75, 0.75 \rightarrow 3.25)$ for $L_x \times L_y = 3 \times 5$. (c) The y -direction spectral flow for $N_b = 10$, $L_x \times L_y = 3 \times 5$, $\phi = 1/3$ with the same branch cut as in (a). (d) The y -direction spectral flow for $N_b = 10$, $L_x \times L_y = 3 \times 5$, $\phi = 1/3$ with the same branch cuts as in (b). (e) The energy spectrum at $\nu = 3/2$ with one pair of defects. The branch cut is located at $(0.25, 0.5 \rightarrow 2.5)$ for $L_x \times L_y = 3 \times 4$.

$g = M + 1$ surface with degeneracy $\mathcal{D}_M^{k=1} = 2^{M+1}$.

The effect of defects is even more intriguing at higher k 's for which host systems have intrinsic non-Abelian topological orders. In this case, unlike the situation with $k = 1$, one pair of defects already leads to a nontrivial enhancement of the ground-state degeneracy. For example, in the case of $k = 2$, the ground state in the absence of defects is two copies of Moore-Read states on the torus, with a degeneracy $\mathcal{D} = 9$ for even $N_b/2$ and $\mathcal{D} = 1$ for odd $N_b/2$. Strikingly, after adding only one pair of defects, we observe an enhanced topological degeneracy of ten-fold for all even N_b , which becomes better for larger system sizes and is robust under twisted boundary conditions [Figs. 4(a) and (c)]. By just adding another pair of defects, the ground-state degeneracy is further enhanced to $\mathcal{D} = 36$ [Figs. 4(b) and (d)], with a faster growth rate than the $k = 1$ case. The dependence of the topological degeneracy on the number of defects convincingly suggests that, by introducing M pairs of defects for $k = 2$, we indeed realize the $\nu = 1$ Moore-Read state on a single $g = M + 1$ surface with degeneracy $\mathcal{D}_M^{k=2} = 2^M(2^{M+1} + 1)$ [38]. A similar enhancement of the topological degeneracy is also observed for $k = 3$, where the ground-state degeneracy is increased from $\mathcal{D} = 16$ to $\mathcal{D} = 20$ by adding $M = 1$ pair of defects [Figs. 4(e)], which is consistent with the $\nu = 3/2$ \mathcal{Z}_3 RR state on a single $g = M + 1$ surface with degeneracy $\mathcal{D}_M^{k=3} = 2[(5 + \sqrt{5})^M + (5 - \sqrt{5})^M]$ [38].

The enhanced topological degeneracy strongly indicates that the defects in our systems can indeed be thought of as genons. In particular, each genon (or defect) in our model carries a distinct nontrivial quantum dimension $d = \lim_{M \rightarrow \infty} (\mathcal{D}_M)^{\frac{1}{2M}}$, i.e., its average contribution to the total degeneracy in the thermodynamic limit differs from that of intrinsic quasiparticles of the host state. For example, we have non-Abelian genons with $d = \sqrt{2}$ at $\nu = 1/2$, although the Laughlin state only has Abelian quasiparticles. More saliently, genons at $\nu = 1$ in our model have $d = 2$ thus allowing for universal quantum computation, while the quasiparticles of Moore-Read state itself cannot [12, 22]. Moreover, we obtain genons with even higher quantum dimension

$d = \sqrt{5 + \sqrt{5}}$ at $\nu = 3/2$. These differences, together with the distinctive projective braiding statistics of defects [12], imply the possibility that genons are more powerful tools for topological quantum computation than ordinary quasiparticles.

Discussion. In this work, we condense the beautiful idea of genons from topological field theory into a recipe for realistic microscopic lattice models. We identify a number of different lattice genons in both Abelian and non-Abelian host states based on their numerically observed defect-induced enhancement of the ground-state degeneracy, which can be thought of as adding genons into the system. The key ingredients of our proposal are already experimentally available and their combined synthesis is plausibly within reach — especially for coupled Laughlin states emerging from a particularly simple onsite two-body interaction. Artificial gauge fields generated by lattice shaking techniques are compatible with multiple internal degrees of freedom as we require. The long-range hopping, which is chosen for theoretical elegance and numerical efficiency, is in fact not essential for the existence of lattice genons [27]. Hence the already realized Hofstadter model in optical lattices [39, 40] can serve as an eminently promising candidate platform for creating genons, while its higher Chern bands provide an additional variety of host quantum Hall liquids [41, 42]. In particular, a recent realization [43] based on a quantum gas microscope already allows single-site addressing, and could be combined with holographic beam shaping methods [44] that provide a natural route towards producing the branch cuts and local potentials necessary to realize lattice genons as we envision.

Acknowledgments. We thank N.R. Cooper and J. Behrmann for useful discussions. Z.L. was supported by Alexander von Humboldt Research Fellowship for Postdoctoral Researchers and the US Department of Energy, Office of Basic Energy Sciences through Grant No. DE-SC0002140. The latter was specifically for the use of computational facilities at Princeton University. G.M. is supported by The Royal Society – Grant No. UF120157, and acknowledges use of the Darwin Supercomputer of

the University of Cambridge High Performance Computing Service, funded by Strategic Research Infrastructure Funding from the Higher Education Funding Council for England and funding from the Science and Technology Facilities Council. E.J.B. was supported by the Swedish research council (VR) and the Wallenberg Academy Fellows program of the Knut and Alice Wallenberg Foundation.

* Corresponding author: G.Moller@kent.ac.uk; These authors contributed equally to the inception of this project.

† These authors contributed equally to the inception of this project.

- [1] R. B. Laughlin, *Anomalous Quantum Hall Effect: An Incompressible Quantum Fluid with Fractionally Charged Excitations*, *Phys. Rev. Lett.* **50**, 1395 (1983).
- [2] X. G. Wen, *Topological orders and Chern-Simons theory in strongly correlated quantum liquid*, *Int. J. Mod. Phys. B*, **05**, 1641 (1991).
- [3] G. Moore and N. Read, *Nonabelions in the fractional quantum hall effect*, *Nucl. Phys. B* **360**, 362 (1991).
- [4] M. Oshikawa and T. Senthil, *Fractionalization, Topological Order, and Quasiparticle Statistics*, *Phys. Rev. Lett.* **96**, 060601 (2006).
- [5] J. Maciejko and G. A. Fiete, *Fractionalized topological insulators*, *Nat. Phys.*, **11**, 385 (2015).
- [6] H. Bombin, *Topological Order with a Twist: Ising Anyons from an Abelian Model*, *Phys. Rev. Lett.* **105**, 030403 (2010).
- [7] J. C. Y. Teo and C. L. Kane, *Majorana Fermions and Non-Abelian Statistics in Three Dimensions*, *Phys. Rev. Lett.* **104**, 046401 (2010).
- [8] M. Freedman, M. B. Hastings, C. Nayak, X.-L. Qi, K. Walker, and Z. Wang, *Projective ribbon permutation statistics: A remnant of non-Abelian braiding in higher dimensions*, *Phys. Rev. B* **83**, 115132 (2011).
- [9] N. H. Lindner, E. Berg, G. Refael, and A. Stern, *Fractionalizing Majorana Fermions: Non-Abelian Statistics on the Edges of Abelian Quantum Hall States*, *Phys. Rev. X* **2**, 041002 (2012).
- [10] Y.-Z. You and X.-G. Wen, *Projective non-Abelian statistics of dislocation defects in a Z_N rotor model*, *Phys. Rev. B* **86**, 161107 (2012).
- [11] M. Barkeshli and X.-L. Qi, *Topological Nematic States and Non-Abelian Lattice Dislocations*, *Phys. Rev. X* **2**, 031013 (2012).
- [12] M. Barkeshli, C.-M. Jian, and X.-L. Qi, *Twist defects and projective non-Abelian braiding statistics*, *Phys. Rev. B* **87**, 045130 (2013).
- [13] M. Barkeshli, C.-M. Jian, and X.-L. Qi, *Theory of defects in Abelian topological states*, *Phys. Rev. B* **88**, 235103 (2013).
- [14] Y.-Z. You, C.-Ming Jian, and X.-G. Wen, *Synthetic non-Abelian statistics by Abelian anyon condensation*, *Phys. Rev. B* **87**, 045106 (2013).
- [15] B. J. Brown, S. D. Bartlett, A. C. Doherty, and S. D. Barrett, *Topological Entanglement Entropy with a Twist*, *Phys. Rev. Lett.* **111**, 220402 (2013).
- [16] J. Fuchs and C. Schweigert, *A Note on Permutation Twist Defects in Topological Bilayer Phases*, *Lett. Math. Phys.* **104**, 1385 (2014).
- [17] M. Barkeshli, H.-C. Jiang, R. Thomale, and X.-L. Qi, *Generalized Kitaev Models and Extrinsic Non-Abelian Twist Defects*, *Phys. Rev. Lett.* **114**, 026401 (2015).
- [18] H. Zheng, A. Dua, and L. Jiang, *Demonstrating non-Abelian statistics of Majorana fermions using twist defects*, *Phys. Rev. B* **92**, 245139 (2015).
- [19] Yizhi You and Yi-Zhuang You, *Geometry defects in bosonic symmetry-protected topological phases*, *Phys. Rev. B* **93**, 245135 (2016).
- [20] A. Bühler, *et al.*, *Majorana modes and p-wave superfluids for fermionic atoms in optical lattices*, *Nat. Comm.* **5**, 4504 (2014).
- [21] A. Y. Kitaev, *Fault-tolerant quantum computation by anyons*, *Ann. Phys.* **303**, 2 (2003).
- [22] C. Nayak, S. H. Simon, A. Stern, M. Freedman, and S. Das Sarma, *Non-Abelian anyons and topological quantum computation*, *Rev. Mod. Phys.* **80**, 1083 (2008).
- [23] S. A. Parameswaran, R. Roy, and S. L. Sondhi, *Fractional quantum Hall physics in topological flat bands*, *C. R. Physique* **14**, 816 (2013).
- [24] E.J. Bergholtz and Z. Liu, *Topological Flat Band Models and Fractional Chern Insulators*, *Int. J. Mod. Phys. B* **27**, 1330017 (2013).
- [25] E. Kapit and E. Mueller, *Exact Parent Hamiltonian for the Quantum Hall States in a Optical Lattice*, *Phys. Rev. Lett.* **105**, 215303 (2010).
- [26] In a finite system with periodic boundary conditions, both the lattice sites and defects appear periodically. To adjust Eq. (1) to periodic boundary conditions, we replace $t(z_j, z_k)$ by $\sum_{s,t=-\infty}^{+\infty} t(z_j + sL_x\mathbf{e}_x + tL_y\mathbf{e}_y, z_k)e^{2\pi i sL_x y_j \phi}$, and in n_{jk} we count all crossings between the hopping from z_k to $z_j + sL_x\mathbf{e}_x + tL_y\mathbf{e}_y$ and the periodically appearing branch cuts. Twisted boundary conditions can be implemented by replacing $t(z_j, z_k)$ by $\sum_{s,t=-\infty}^{+\infty} t(z_j + sL_x\mathbf{e}_x + tL_y\mathbf{e}_y, z_k)e^{2\pi i sL_x y_j \phi} e^{i s \Phi_x} e^{i t \Phi_y}$.
- [27] See the Supplementary Material for short-range hopping tight-binding models and tilted branch cuts.
- [28] Z. Liu, E. J. Bergholtz and E. Kapit, *Non-Abelian fractional Chern insulators from long-range interactions*, *Phys. Rev. B* **88**, 205101 (2013).
- [29] J. Behrmann, Z. Liu, and E.J. Bergholtz, *Model Fractional Chern Insulators*, *Phys. Rev. Lett.* **116**, 216802 (2016).
- [30] X.-G. Wen, and A. Zee, *Shift and spin vector: New topological quantum numbers for the Hall fluids*, *Phys. Rev. Lett.* **69**, 953 (1992).
- [31] For a fractional quantum Hall state at filling fraction ν in the lowest Landau level on a surface of genus g , we have $N_\phi = N/\nu - S_g$, where N_ϕ is the number of magnetic flux quanta penetrating the surface related to the number of single-particle states N_s in the lowest Landau level by $N_s = N_\phi + 1 - g$ [30], N is the number of particles, and $S_g = S_{g=0} \times (1 - g)$ is the so-called topological shift [30]. For $\nu = k/2$ \mathcal{Z}_k bosonic RR states, by setting $S_{g=0} = 2$, we have $N_s = 2N/k - (1 - g)$ as shown in Eq. (3).
- [32] We pursue a good separation of scales in the many-body spectrum when we choose the locations of defects. However, we emphasize that our results are not sensitive to the precise locations of defects or the arrangement of branch cuts and crucially also hold for models including only short-range hopping once the system size is large enough [27].
- [33] Taking the two-body on-site interaction as an example, the interaction after projection is $H_{\text{int}}^{\text{proj}} = \sum_{m_1, m_2, m_3, m_4=1}^{2\phi L_x L_y + M} C_{m_1, m_2, m_3, m_4} a_{m_1}^\dagger a_{m_2}^\dagger a_{m_3} a_{m_4}$ with $C_{m_1, m_2, m_3, m_4} = \sum_{i=1}^{2L_x L_y} \psi_{m_1, i}^* \psi_{m_2, i} \psi_{m_3, i} \psi_{m_4, i}$, where a_m^\dagger (a_m) creates (annihilates) a boson on the eigenstate ψ_m of H_0 , and $\psi_m = (\psi_{m,1}, \dots, \psi_{m,2L_x L_y})$ in the lattice site basis

- $a_{j,\sigma}^\dagger|\text{vacuum}\rangle$.
- [34] N. Regnault and B. A. Bernevig, *Fractional Chern Insulator*, *Phys. Rev. X* **1**, 021014 (2011).
- [35] A. Sterdyniak, N. Regnault, and B. A. Bernevig, *Extracting Excitations from Model State Entanglement*, *Phys. Rev. Lett.* **106**, 100405 (2011).
- [36] For a \mathcal{D} -fold degenerate ground-state manifold $\{|\Psi_\alpha\rangle\}$ of N particles, we define the PES levels ξ as $\xi \equiv -\ln \lambda$, where the λ 's are the eigenvalues of the reduced density matrix ρ_A of N_A particles obtained by tracing out $N_B = N - N_A$ particles from the whole system, i.e., $\rho_A = \text{Tr}_B \rho$ with $\rho = \frac{1}{\mathcal{D}} \sum_{\alpha=1}^{\mathcal{D}} |\Psi_\alpha\rangle\langle\Psi_\alpha|$. A gap in the PES is expected, below which the number of PES levels is the same as the counting of the corresponding quasihole excitation spectrum [34], which in our case can be obtained from diagonalizing the interaction Hamiltonian of N_b^A particles on the same lattice size.
- [37] A. Sterdyniak, N. Regnault, and G. Möller, *Particle entanglement spectra for quantum Hall states on lattices*, *Phys. Rev. B* **86**, 165314 (2012).
- [38] E. Ardonne, E. Bergholtz, J. Kailasvuori, and E. Wikberg, *Degeneracy of non-Abelian quantum Hall states on the torus: domain walls and conformal field theory*, *J. Stat. Mech.* P04016 (2008).
- [39] M. Aidelsburger, M. Atala, M. Lohse, J. T. Barreiro, B. Paredes, and I. Bloch, *Realization of the Hofstadter Hamiltonian with Ultracold Atoms in Optical Lattices*, *Phys. Rev. Lett.* **111**, 185301 (2013).
- [40] H. Miyake, G. A. Siviloglou, C. J. Kennedy, W. C. Burton, and W. Ketterle, *Realizing the Harper Hamiltonian with Laser-Assisted Tunneling in Optical Lattices*, *Phys. Rev. Lett.* **111**, 185302 (2013).
- [41] G. Möller, N. R. Cooper, *Composite Fermion Theory for Bosonic Quantum Hall States on Lattices*, *Phys. Rev. Lett.* **103**, 105303 (2009).
- [42] G. Möller, N. R. Cooper, *Fractional Chern Insulators in Harper-Hofstadter Bands with Higher Chern Number*, *Phys. Rev. Lett.* **115**, 126401 (2015).
- [43] M. E. Tai, A. Lukin, M. Rispoli, R. Schittko, T. Menke, D. Borgnia, P. M. Preiss, F. Grusdt, A. M. Kaufman, M. Greiner, *Microscopy of the interacting Harper-Hofstadter model in the few-body limit*, [arXiv:1612.05631](https://arxiv.org/abs/1612.05631).
- [44] P. Zupancic, P. M. Preiss, R. Ma, A. Lukin, M. E. Tai, M. Rispoli, R. Islam, and M. Greiner, *Ultra-precise holographic beam shaping for microscopic quantum control*, *Opt. Express* **24**, 13881 (2016).

SUPPLEMENTARY MATERIAL

Short-range hopping. In the main text, we use a tight-binding Hamiltonian with local but long-range hopping for theoretical elegance. Now we show that we can obtain similar results with only short-range hopping.

We only keep the nearest-neighbor and next-nearest-neighbor hopping in the tight-binding model, Eq. (1) in the main text. Thus, we obtain a new tight-binding model with short-range hopping

$$H'_0 = \sum_{j,k,\sigma} t'(z_j, z_k) a_{j, \mathcal{F}^{n_{jk}}(\sigma)}^\dagger a_{k,\sigma}, \quad (\text{S1})$$

where $t'(z_j, z_k) = (-1)^{x+y+xy} e^{-\frac{\pi}{2}(1-\phi)|z|^2} e^{-i\pi\phi(x_j+x_k)y}$ for $|z|^2 \leq 2$ and $t'(z_j, z_k) = 0$ for $|z|^2 > 2$. The meanings of the symbols are the same as those in the main text.

Although the exact flatness of the lowest $2\phi L_x L_y$ eigenstates in the absence of defects is lost due to the hopping truncation, we still find that defects have almost the same effect on the band structure of H'_0 as that on H_0 shown in the main text [Figs. S1 and S2]. The energies of some eigenstates localized near the defects deviate from the original bands, and the dispersion of the lowest $2\phi L_x L_y + M$ eigenstates can be reduced by a local potential $V = -\sum_{n=1}^{2\phi L_x L_y + M} \epsilon_n \mathcal{T}_R(|\psi_n\rangle\langle\psi_n|)$, where ϵ_n 's and ψ_n 's are now the eigenvalues and eigenvectors of H'_0 respectively. One can notice that such a flattening procedure works better for smaller ϕ [Figs. S1 and S2].

We diagonalize the interaction projected onto the lowest $2\phi L_x L_y + M$ eigenstates of H'_0 to examine the topological degeneracy at various filling fractions. Strikingly, we can get the expected topological degeneracy even though we have truncated the hopping [Fig. S3]. Moreover, we find that the eight-fold Laughlin degeneracy remains stable for small ϕ even if we further truncate the hopping range to only the nearest-neighbor sites (yielding the conventional Hofstadter model) [Fig. S4]. These results imply that the long-range hopping is not necessary for the realization of lattice genons, thus facilitating their experimental realization. A realization based on the nearest-neighbor Hofstadter model would provide an additional range of host states to explore, as single layers can be chosen to realize higher Chern number \mathcal{C} bands that support a series of hierarchy states at filling factors $\nu = r/(k\mathcal{C}r + 1)$, with $r \in \mathbb{Z}$ and k even (odd) for bosons (fermions) [42].

Tilted branch cuts. In the main text, we arrange branch cuts in the y -direction. Here, we consider more general locations of defects that yield tilted branch cuts. In general, we denote the branch cut connecting a pair of defects at (X_1, Y_1) and (X_2, Y_2) as $(X_1, Y_1) \rightarrow (X_2, Y_2)$. In the following we use the same tight-binding model H_0 as in the main text.

With tilted branch cuts, we observe a similar effect of defects on the band structure as that in the main text [Fig. S5]. Moreover, the many-body spectra reproduce the expected topological degeneracy for the given number of branch cuts [Fig. S6].

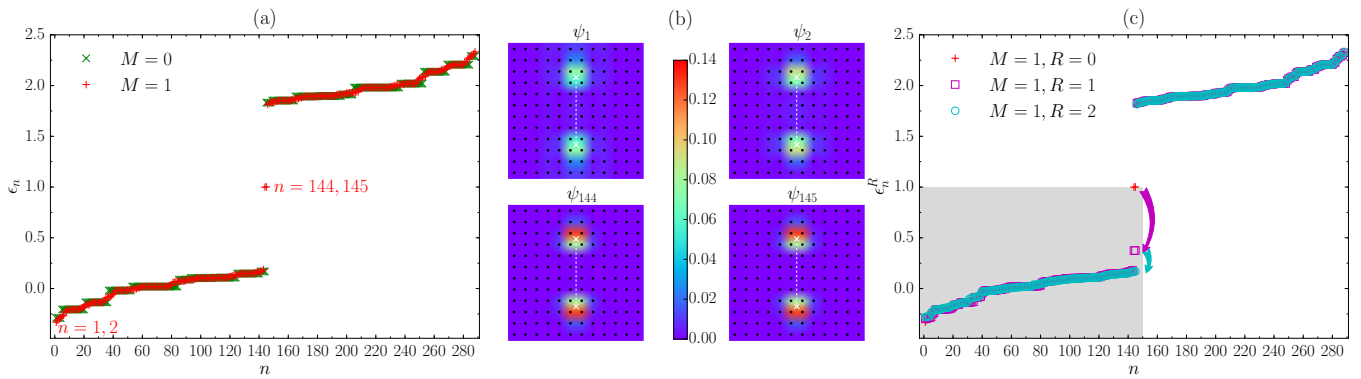


Figure S1. Single-particle spectra and defect-induced localized states with NN and NNN hoppings only. We study the band structure on a $L_x \times L_y = 12 \times 12$ lattice with $\phi = 1/2$. (a) The single-particle spectrum $\{\epsilon_n\}$ of H'_0 . In the absence of defects ($M = 0$), $\epsilon_1, \dots, \epsilon_{144}$ are no longer exactly degenerate at zero energy. With a branch cut ($M = 1$, white dashed line) at $(5.5, 2.5 \rightarrow 8.5)$, the original band structure is distorted, with one nearly degenerate cluster ($\epsilon_{144}, \epsilon_{145}$) having the largest deviation. (b) The lattice site weight of eigenvectors $\psi_1, \psi_2, \psi_{144}, \psi_{145}$ of H'_0 for the same defects as in (a). All of them are strongly localized near the defects. However, the localization of ψ_1 and ψ_2 is weaker than the case of H_0 in the main text, probably because now they have much less energy deviation from the original band structure. (c) The single-particle spectrum $\{\epsilon_n^R\}$ of $H'_0 + V$ with $R = 0, 1$, and 2 and the same defects as in (a). The degeneracy of $\epsilon_1^R, \dots, \epsilon_{145}^R$ (shaded in gray) becomes better for larger R , with the flatness $0.6, 2.2, 3.7$ for $R = 0, 1, 2$.

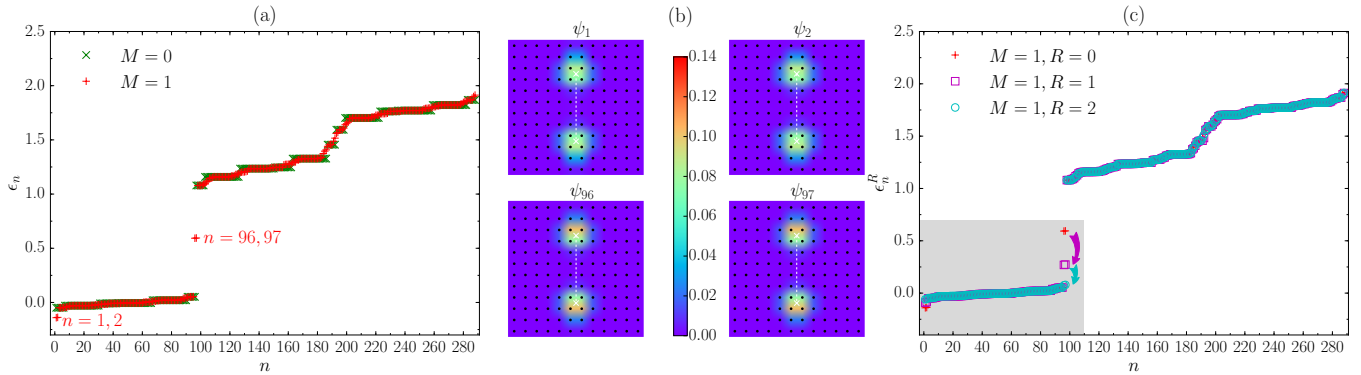


Figure S2. Single-particle spectra and defect-induced localized states with NN and NNN hoppings only. We show the band structure on a $L_x \times L_y = 12 \times 12$ lattice with $\phi = 1/3$. (a) The single-particle spectrum $\{\epsilon_n\}$ of H'_0 . In the absence of defects ($M = 0$), $\epsilon_1, \dots, \epsilon_{96}$ are no longer exactly degenerate at zero energy. With a branch cut ($M = 1$, white dashed line) at $(5.5, 2.5 \rightarrow 8.5)$, the original band structure is distorted, with two nearly degenerate clusters (ϵ_1, ϵ_2) and ($\epsilon_{96}, \epsilon_{97}$) having the largest deviation. (b) The lattice site weight of eigenvectors $\psi_1, \psi_2, \psi_{96}, \psi_{97}$ of H'_0 for the same defects as in (a). All of them are strongly localized near the defects. (c) The single-particle spectrum $\{\epsilon_n^R\}$ of $H'_0 + V$ with $R = 0, 1$, and 2 and the same defects as in (a). The degeneracy of $\epsilon_1^R, \dots, \epsilon_{97}^R$ (shaded in gray) becomes better for larger R , with the flatness $0.7, 2.2, 7.3$ for $R = 0, 1, 2$.

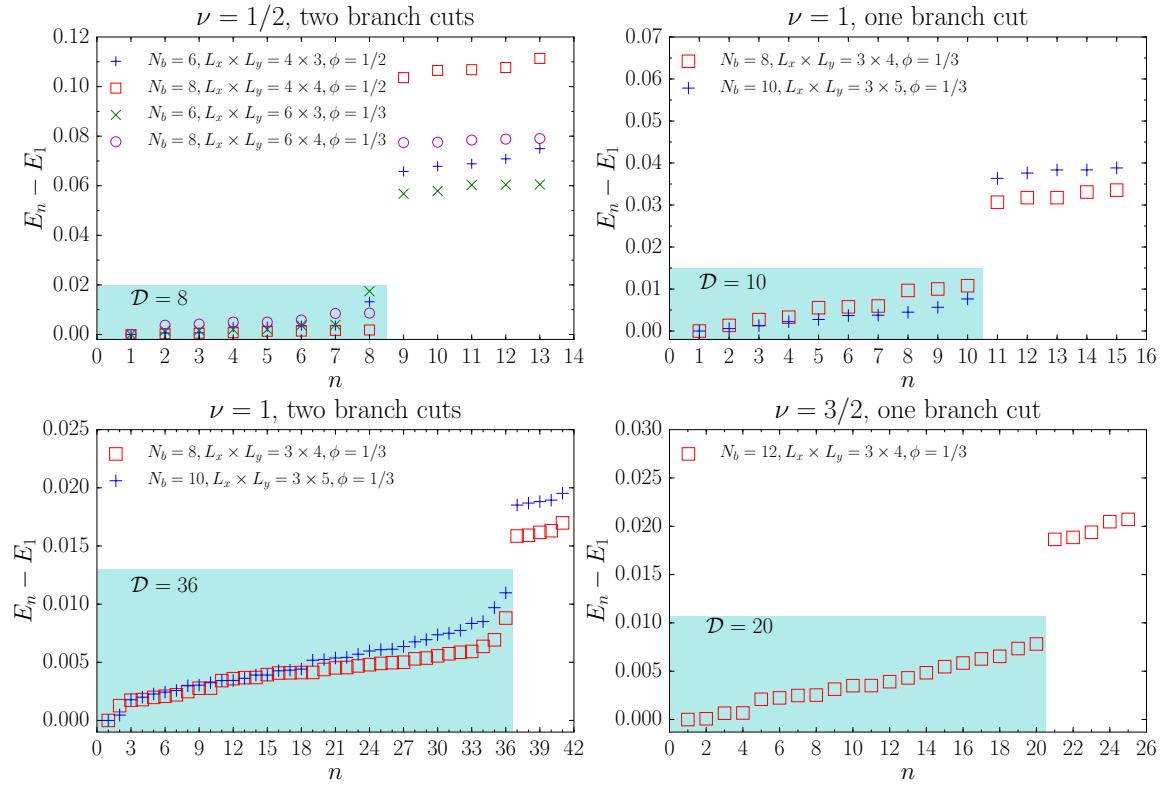


Figure S3. **Defect-enhanced topological degeneracy with NN and NNN hoppings only.** We show the many-body spectra resulting from the single-particle Hamiltonian H'_0 . The interactions and branch cut locations in each specific system size are the same as those used in the main text with H_0 . The approximately degenerate ground states, together with the degeneracy \mathcal{D} , are highlighted by the cyan shade. One can notice that we get the same topological degeneracy as that in the main text.

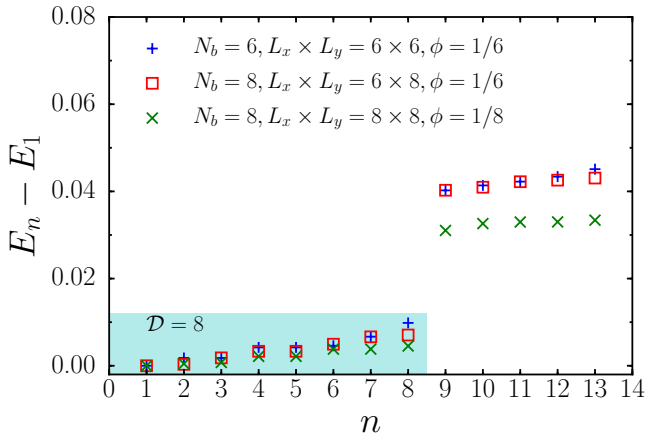


Figure S4. **Defect-enhanced topological degeneracy in the Hofstadter model, for the Abelian $\nu = 1/2$ state.** We show the many-body calculations with the Hofstadter single-particle Hamiltonian for two branch cuts at $\nu = 1/2$. Two branch cuts are located at $(0.25, 0.5 \rightarrow 3.5)$, $(3.25, 0.5 \rightarrow 3.5)$ for $L_x \times L_y = 6 \times 6$; $(0.25, 1.5 \rightarrow 5.5)$, $(3.25, 1.5 \rightarrow 5.5)$ for $L_x \times L_y = 6 \times 8$; and $(1.5, 1.5 \rightarrow 5.5)$, $(5.5, 1.5 \rightarrow 5.5)$ for $L_x \times L_y = 8 \times 8$.

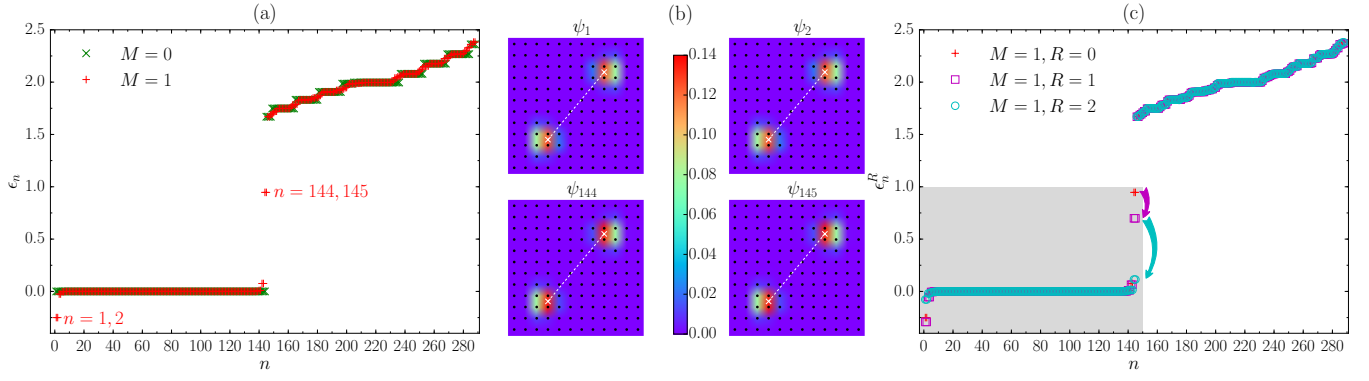


Figure S5. Single-particle spectra and defect-induced localized states for tilted branch cuts. We study the band structure on a $L_x \times L_y = 12 \times 12$ lattice with $\phi = 1/2$. (a) The single-particle spectrum $\{\epsilon_n\}$ of H_0 . In the absence of defects ($M = 0$), $\epsilon_1, \dots, \epsilon_{144}$ are exactly degenerate at zero energy. With a tilted branch cut ($M = 1$, white dashed line) at $(3, 2.5) \rightarrow (8, 8.5)$, the original band structure is distorted, with two nearly degenerate clusters (ϵ_1, ϵ_2) and ($\epsilon_{144}, \epsilon_{145}$) having the largest deviation. (b) The lattice site weight of eigenvectors $\psi_1, \psi_2, \psi_{144}, \psi_{145}$ of H_0 for the same defects as in (a). All of them are strongly localized near the defects. The eigenstates with less energy deviation from the original band structure, for example, $\psi_3, \psi_4, \psi_{142}, \psi_{143}$, are less localized (not shown here). (c) The single-particle spectrum $\{\epsilon_n^R\}$ of $H_0 + V$ with $R = 0, 1$, and 2 and the same defects as in (a). The degeneracy of $\epsilon_1^R, \dots, \epsilon_{145}^R$ (shaded in gray) becomes better for larger R , with the flatness $0.6, 1.0, 8.1$ for $R = 0, 1, 2$.

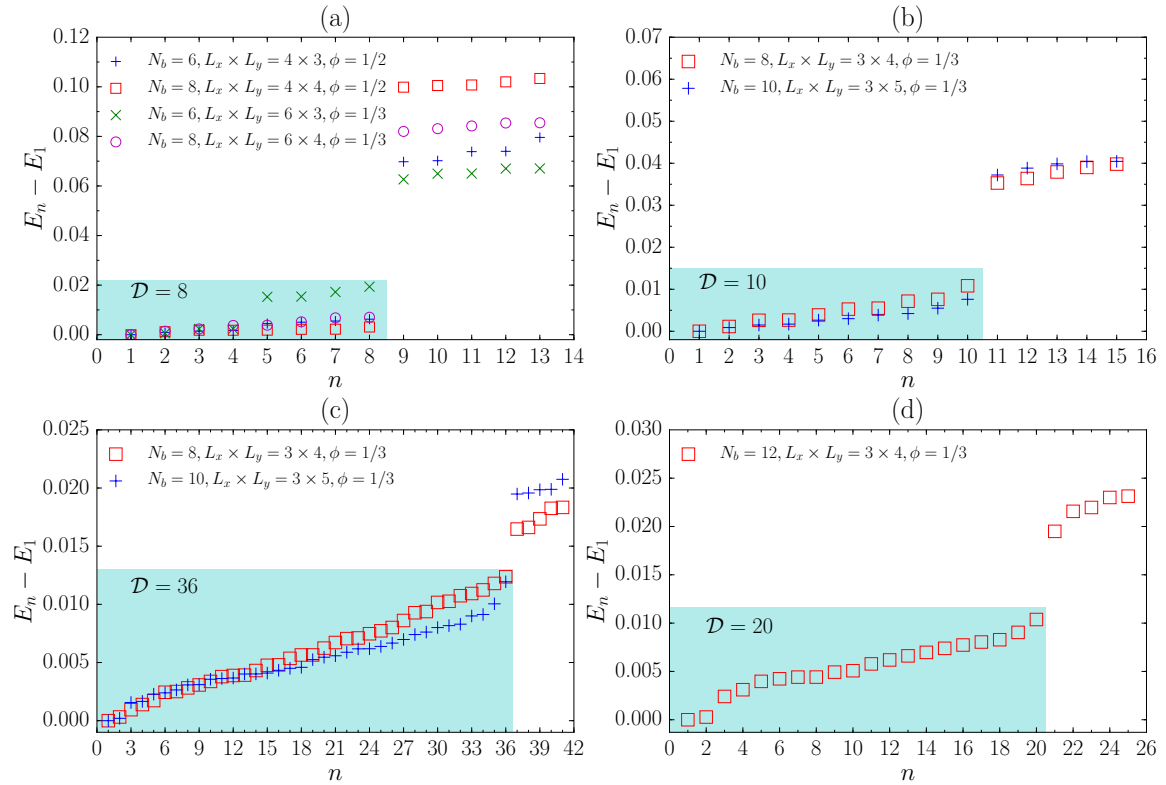


Figure S6. Many-body spectra for tilted branch cuts. The approximately degenerate ground states, together with the degeneracy \mathcal{D} , are highlighted by the cyan shade. (a) $\nu = 1/2$ with two branch cuts at $(0.25, 0.5) \rightarrow (0.5, 2), (2.25, 0) \rightarrow (2.5, 1.5)$ for $L_x \times L_y = 4 \times 3$; $(0, 0.75) \rightarrow (1, 2.75), (2, 0.25) \rightarrow (3, 2.25)$ for $L_x \times L_y = 4 \times 4$; $(0.25, 0.5) \rightarrow (0.5, 2), (3.25, 0) \rightarrow (3.5, 1.5)$ for $L_x \times L_y = 6 \times 3$; and $(0.5, 0.75) \rightarrow (1.5, 2.75), (3.5, 0.25) \rightarrow (4.5, 2.25)$ for $L_x \times L_y = 6 \times 4$. (b) $\nu = 1$ with one branch cut at $(0.25, 0.5) \rightarrow (1.75, 2.5)$ for $L_x \times L_y = 3 \times 4$ and $(0.25, 0.5) \rightarrow (1.75, 3)$ for $L_x \times L_y = 3 \times 5$. (c) $\nu = 1$ with two branch cuts at $(0.1, 0.75) \rightarrow (0.4, 2.75), (1.6, 0.25) \rightarrow (1.9, 2.25)$ for $L_x \times L_y = 3 \times 4$ and $(0.19, 0.5) \rightarrow (0.31, 3.5), (1.69, 0.45) \rightarrow (1.81, 3.45)$ for $L_x \times L_y = 3 \times 5$. (d) $\nu = 3/2$ with one branch cut at $(0.5, 0.5) \rightarrow (2, 2.5)$ for $L_x \times L_y = 3 \times 4$.